

Automated Backbone NMR Resonance Assignment of Large Proteins Using Redundant Linking from a Single Simultaneous Acquisition

Jan Stanek,[#] Tobias Schubeis,[#] Piotr Paluch, Peter Güntert, Loren B. Andreas, and Guido Pintacuda*



Cite This: *J. Am. Chem. Soc.* 2020, 142, 5793–5799



Read Online

ACCESS |



Metrics & More

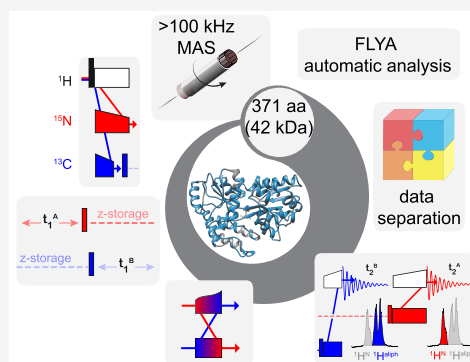


Article Recommendations



Supporting Information

ABSTRACT: Thanks to magic-angle spinning (MAS) probes with frequencies of 60–100 kHz, the benefit of high-sensitivity ^1H detection can now be broadly realized in biomolecular solid-state NMR for the analysis of microcrystalline, sedimented, or lipid-embedded preparations. Nonetheless, performing the assignment of all resonances remains a rate-limiting step in protein structural studies, and even the latest optimized protocols fail to perform this step when the protein size exceeds ~ 20 kDa. Here, we leverage the benefits of fast (100 kHz) MAS and high (800 MHz) magnetic fields to design an approach that lifts this limitation. Through the creation, conservation, and acquisition of independent magnetization pathways within a single triple-resonance MAS NMR experiment, a single self-consistent data set can be acquired, providing enhanced sensitivity, reduced vulnerability to machine or sample instabilities, and highly redundant linking that supports fully automated peak picking and resonance assignment. The method, dubbed RAVASSA (redundant assignment via a single simultaneous acquisition), is demonstrated with the assignment of the largest protein to date in the solid state, the 42.5 kDa maltose binding protein, using a single fully protonated microcrystalline sample and 1 week of spectrometer time.



INTRODUCTION

The proton is inherently the most sensitive nuclear spin because it has the highest gyromagnetic ratio among all stable isotopes. This is recognized in solution NMR spectroscopy, where standard acquisition schemes are centered around amide protons for protein resonance assignment and structure determination. For solid-state NMR, following years of pioneering developments,^{2–5} the benefit of high-sensitivity ^1H detection can now be broadly realized thanks to magic-angle spinning (MAS) probes with frequencies of 60–100 kHz^{6,7} and beyond.⁸ With these advances in instrumentation, high-resolution “fingerprint” correlation spectra can now be obtained for deuterated^{9,10} and fully protonated proteins^{11,12} and RNA¹³ within minutes using a submilligram sample quantity. This has led to the development of a palette of triple-resonance experiments for accelerating the sequential assignment^{1,14–17} and expanding the repertoire of proteins for which a nearly complete resonance assignment can be obtained. Currently, however, the complexity of spectra in solids permits the analysis of microcrystalline, sedimented, or lipid-embedded preparations of small proteins, and only a few examples above 250 amino acid residues (aa) were reported, for which either deuteration^{18–21} and/or a combination of differently labeled samples^{12,22–24} was required.

A potential solution to overcome this size barrier is provided by the study of fully protonated proteins at 100 kHz MAS and

above, with the design of complementary approaches based on the detection of narrow α -proton resonances.^{25,26} However, the acquisition of such an expanded data set also approximately doubles the spectrometer time required, which makes the entire acquisition vulnerable to machine or sample instabilities,²⁷ and increases severely the complexity of the data analysis. Deviations in peak position exceeding the line width are not unusual in these approaches, in particular, if multiple samples are analyzed. Although these deviations can sometimes be recognized by expert manual analysis, they can be catastrophic for automated approaches, which rely on strict resonance matching thresholds.²⁸ With a manual approach, assignment of thousands of resonances is cumbersome and time-consuming, commonly demanding years of data analysis. We show in the following that these issues can be addressed by automated analysis of a single self-consistent data set composed of six simultaneously acquired ^1H -detected three-dimensional (3D) spectra employing MAS at frequencies exceeding 100 kHz. The method, hereafter dubbed redundant

Received: January 8, 2020

Published: March 4, 2020



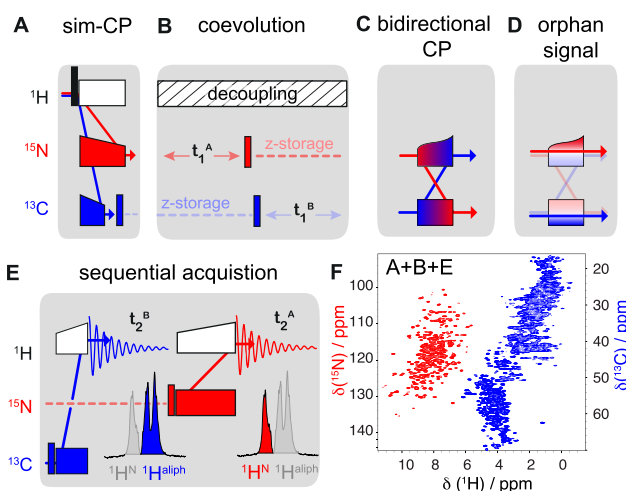


Figure 1. Scheme of radiofrequency (RF) building blocks for multiple pathway coherence transfers: (A) simultaneous cross-polarization (CP) of amide ^{15}N and $^{13}\text{C}\alpha$ spins from spatially proximal protons; (B) unconstrained coevolution of ^{15}N and ^{13}C chemical shifts; (C) bidirectional ^{15}N – ^{13}C CP without and (D) with recovery of orphan coherence; (E) a single scan sequential acquisition of α and amide ^1H signal following respective CPs from $^{13}\text{C}\alpha$ and ^{15}N . (F) Simultaneous dipolar-based ^{13}C , ^{15}N -HSQC spectrum of maltose binding protein (see Supporting Information for a detailed RF scheme of this experiment).

assignment via a single simultaneous acquisition (RAVASSA), enhances sensitivity, with a 2–3-fold reduction in experimental time, and results in spectra that support fully automated peak picking and resonance assignment. We demonstrate its efficiency with the 371 aa maltose binding protein (MBP), using a single fully protonated sample (<1 mg of uniformly ^{13}C , ^{15}N -labeled material).

RESULTS

Figure 1 depicts the key building blocks needed to implement RAVASSA, by creating, conserving, and recording independent magnetization pathways within a single triple-resonance MAS NMR experiment: (A) simultaneous cross-polarization (SIM-CP) from ^1H to both ^{15}N and ^{13}C ;^{29,30} (B) coevolution (time-sharing) of indirect ^{15}N and ^{13}C chemical shifts;³¹ (C) bidirectional cross-polarization allowing simultaneous polarization transfer from ^{13}C to ^{15}N and vice versa;²⁹ (D) recovery of orphan terms left-over due to incomplete CP transfers;^{32,33} and (E) separated acquisition of $^1\text{H}\alpha$ and $^1\text{H}^{\text{N}}$ signals, one occurring immediately after the other.³³ In panel (F), we show the simplest case of a coacquired CP- ^{13}C , ^{15}N -HSQC^{31,33} spectrum of MBP, which takes advantage of blocks A, B, and E. The amide and aliphatic two-dimensional (2D) correlations were acquired simultaneously in 1 h, as compared to 2 h for recording two separate spectra, on a 800 MHz spectrometer at 107 kHz MAS. Samples with 100% abundance of protons, which recently became available to proton-detected NMR analysis with ≥ 100 kHz MAS, are central to the performance of SIM-CP because they contain independent reservoirs of ^1H magnetization for ^1H - ^{15}N and ^1H - $^{13}\text{C}\alpha$ pathways as demonstrated both experimentally and by quantum-mechanical calculations found in Figures S1–S3 in the Supporting Information. Note that although our main focus here is on the backbone nuclei, simultaneous polarization in fully protonated proteins can also be exploited to generate correlations of side-chain spins, for example, through-space contacts using broad-band ^1H , ^1H RFDR techniques.³¹ Concerning the mode of detection (Figure 1E), deferring the acquisition of $^1\text{H}^{\text{N}}$ signal comes at virtually no cost due to very

slow relaxation of the ^{15}N z-polarization in solids (T_1 on the order of seconds).²⁹ Additionally, simpler radiofrequency (RF) conditions are used for separate “back” CP, and the cross-talk between pathways ($^{15}\text{N} \rightarrow ^1\text{H}\alpha$ and $^{13}\text{C}\alpha \rightarrow ^1\text{H}^{\text{N}}$ transfers) is avoided. Also, $^1\text{H}\alpha$ and $^1\text{H}^{\text{N}}$ signals, with partially overlapping chemical shift ranges, are cleanly separated.

These design principles are used to construct the more complex pulse sequences discussed below. Figure 2 shows the

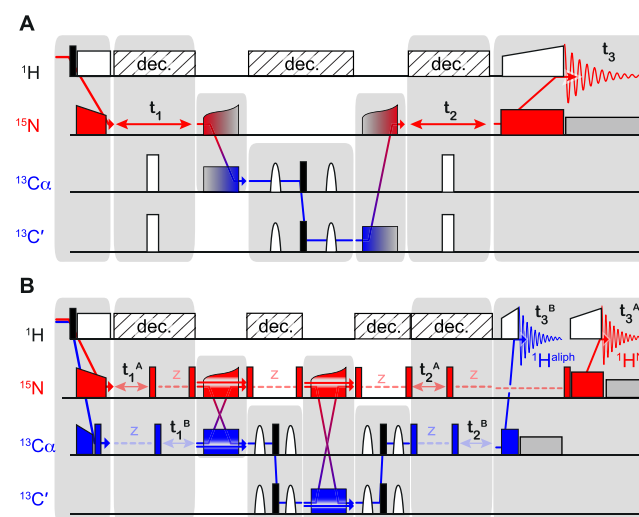


Figure 2. Simplified time diagram of RF irradiation for (A) conventional amide-to-amide proton-transfer experiment (NNH)¹⁵ and (B) its expansion using simultaneous excitation, coevolution, and bidirectional CP transfers (RAVASSA).

pulse sequence for an implementation of RAVASSA that is based around a direct amide-to-amide transfer experiment (NNH).^{15,16} A comparison of panels (A) and (B) shows the additional transfer blocks used to record a total of eight unique transfer pathways. The NNH scheme contains five coherence transfers between consecutive nuclei along the protein

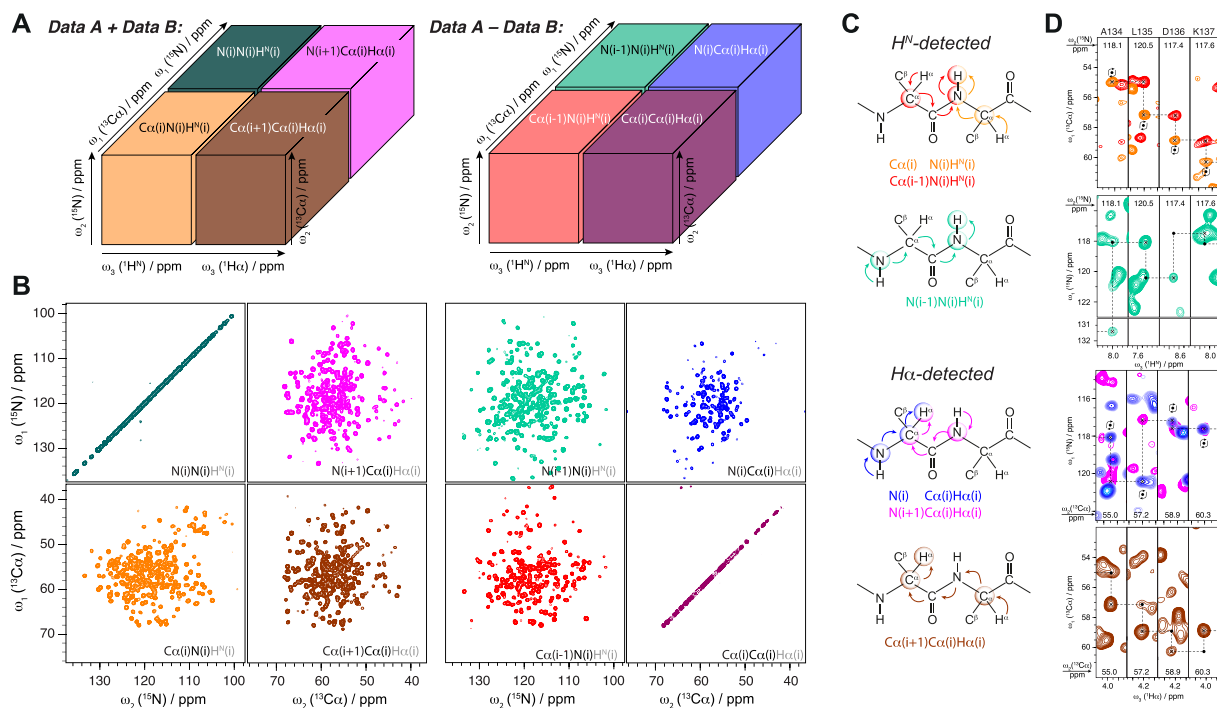


Figure 3. (A) Data layout of eight simultaneously acquired spectra after addition/subtraction of interleaved signals A and B. Separation of pathways undergoing either $^{13}\text{C}\alpha$ or ^{15}N evolution in ω_1 is achieved by a doubled spectral window and TPPI-type up- and downfield frequency shift, whereas separation in ω_2 is unnecessary because the frequency range ($^{13}\text{C}\alpha$ or ^{15}N) is implied from the detected nucleus. (B) Skyline projections of the eight spectra onto the ω_1 - ω_2 plane ($^{13}\text{C}\alpha$ or ^{15}N , and combinations thereof). (C) Scheme of simultaneously observed coherence transfer pathways across the protein backbone that give rise to four independent resonance matching methods. (D) Representative strips showing sequential assignment of ^{15}N , $^{13}\text{C}\alpha$, $^1\text{H}\alpha$, and $^1\text{H}^{\text{N}}$ resonances of residues A134-K137 of MBP based on intra- (orange and blue contours) and interresidue correlations (red and magenta contours) found in six simultaneously acquired 3D spectra employing $^1\text{H}^{\text{N}}$ detection (two top panels, in orange, red, and light green) or $^1\text{H}\alpha$ detection (two bottom panels, in blue, magenta, and brown). For (H)N(CA)(CO)NH (second from the top) and (H)CA(N)(CO)CAHA (bottom last) spectra the implied positions of diagonal peaks (suppressed in these experiments) are shown with dots to illustrate the sequential walk. The ω_1 (either $^{13}\text{C}\alpha$ or ^{15}N)- ω_3 (^1H) cross sections of 3D spectra are shown at the ω_2 (either ^{15}N or $^{13}\text{C}\alpha$) frequency indicated in each strip.

backbone, therefore containing multiple opportunities for the incorporation of the building blocks described above (see the [Supporting Information](#) for a detailed description of the pulse sequences). Simultaneous CP, coevolution, and bidirectional CP naturally lead to acquisition of an analogous experiment for $\text{H}\alpha$ -detected inter-residue $\text{C}\alpha$ - $\text{C}\alpha$ correlation (CCH) together with NNH. Through retaining of the orphan spin operators ([Figure 1D](#)) left after the ^{13}C - ^{15}N CP, four additional spectra (and 2-fold redundant resonance linking, as described below) can be coacquired, namely, the intra- and inter-residue N - $\text{C}\alpha$ - $\text{H}\alpha$ and $\text{C}\alpha$ - N - H^{N} correlations. Overall, a total of six useful pathways can be observed.

[Figure 3](#) shows the resulting eight coacquired spectra, together with representative data on MBP. A proper separation of data sets requires only a doubling of a spectral window in dimension ω_1 , and one additional phase cycle to discriminate pairs of pathways, without any impact on sensitivity. A trivial linear combination of data is used to extract the spectra arranged as shown in [Figure 3A](#). Our implementation makes no compromise on resolution in any dimension because of the possibility of extending periods of low-power proton decoupling during each indirect evolution (see the [Supporting Information](#)). Unconstrained chemical shift evolution times for ^{15}N and ^{13}C nuclei are indeed essential for the resolution of spectra for proteins as large as MBP. The experiment was performed in less than 5 days (instead of more than 16 days

necessary with a regular acquisition) and showed excellent sensitivity, resolution, and high information content, as demonstrated with heteronuclear (ω_1 - ω_2) projections of component spectra in [Figure 3B](#). Together, the 4-fold redundant sequential linking of the resulting data sets provide highly fault-tolerant data for backbone resonance assignment ([Figure 3C](#)). It consists of all combinations: $^1\text{H}^{\text{N}}$ -detected spectra with sequential correlations through (1) $^{13}\text{C}\alpha$ or (2) ^{15}N chemical shifts and, symmetrically, $^1\text{H}\alpha$ -detected spectra correlated by (3) ^{15}N or (4) $^{13}\text{C}\alpha$ frequencies. Representative strips from six spectra are shown in [Figure 3D](#). Completeness of the spectra is characterized by automatic identification of 275–309 cross peaks out of a maximum of 349–371 expected in particular spectra (1770 in total). Peaks were automatically identified using the routine embedded in the spectral analysis software CCPN³⁴ and inevitably contained a certain fraction (approximately 15%) of noise peaks. The redundancy of information and consistency of chemical shifts in four assignment connectivities makes it perfectly amenable to automation and robust in the presence of spurious peaks.

For assignment automation, we turned to the exceptionally flexible automated resonance assignment algorithm FLYA³⁵ that has been applied to $^{13}\text{C}/^{15}\text{N}$ -detected solid-state data³⁶ and very large methyl-labeled proteins.³⁷ The algorithm accommodated unusual $\text{H}\alpha$ -detected correlations with straightforward extensions of the FLYA library (provided in

the Supporting Information). Given the discontinuities in sequential linking due to 21 proline residues (6% of the sequence) or otherwise missing correlations, we expanded our data set by intraresidue (but not inter-residue) correlations of either amide and α -protons to $^{13}\text{C}\beta$ shifts (namely, (H)(CA)-CB(CA)NH³⁸ and (H)(CA)CBCAH²⁵ spectra), which provide reliable information on a specific residue type and thus greatly assist in locating fragments within the protein sequence. As demonstrated in Figure 4, small deviations of

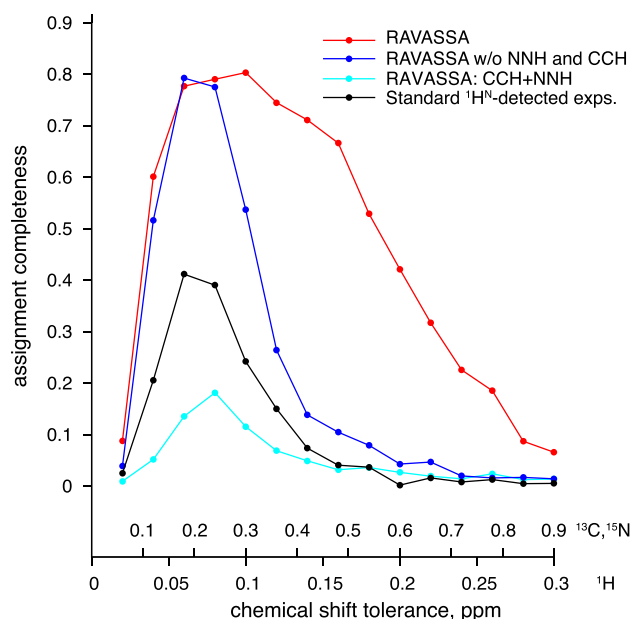


Figure 4. Characterization of the sensitivity of the automated assignment with respect to the matching tolerance. Red, blue, cyan, and black dots indicate the assignment completeness, defined as the ratio of the strongly assigned to all $^1\text{H}^{\text{N}}$, $^1\text{H}\alpha$, $^{13}\text{C}\alpha$, $^{13}\text{C}\beta$, and ^{15}N resonances, obtained with the complete and reduced RAVASSA data sets, as well as with the classical $^1\text{H}^{\text{N}}$ detected data sets,¹ respectively. Points are connected for eye guidance only.

chemical shifts (approximately 0.1 and 0.3 ppm for ^1H and $^{13}\text{C}/^{15}\text{N}$ shifts) and a high redundancy of information allowed to overcome critical ambiguity of resonance matching, typically encountered in large proteins, leading to approximately 82% complete assignment. This is in contrast to the previous state of the art based on the $^1\text{H}^{\text{N}}$ detection and matching of ^{13}C chemical shifts¹ (black curve in Figure 4), which was used to assign a suite of smaller proteins, but fails to assign more than 40% of MBP resonances regardless of matching tolerances. The lower limit for chemical shift tolerances is imposed by experimental line widths and sensitivity, and for many important classes of samples (e.g., for integral membrane or fibrillar proteins), larger line widths typically are found compared to those observed for MBP. It is apparent from Figure 4 that the inherent ambiguity of the large protein MBP is beyond the capability of the five $^1\text{H}^{\text{N}}$ -detected spectra, whereas the new approach leads to robust assignment. This is particularly apparent for higher tolerance values that correspond to the case of increased line widths found for many important biological samples.

To further investigate the key component of RAVASSA, we restricted our data set by independently recording joint intra- and inter-residue N- $\text{C}\alpha$ -H α and $\text{C}\alpha$ -N- H^{N} correlations (pulse

schemes provided in the Supporting Information). This data also benefits from improved chemical shift consistency inherent for simultaneously acquired spectra; thus, the limiting tolerances (lower limit) are identical to those of RAVASSA. In the case of MBP the extent of assignment is almost as good; however, the restricted data set breaks down rapidly with increasing matching tolerance (blue curve in Figure 4). It is therefore clear that the higher robustness of RAVASSA with respect to large line widths stems from the NNH and CCH correlations. Interestingly, these correlations alone are clearly too ambiguous to yield a complete assignment in an automatic way (cyan curve in Figure 4). In FLYA, the four pathways support each other in resolving assignment ambiguities, with a significant cooperative effect (see Figure S12 for statistics on how often peaks from the different pathways are assigned for each residue). A relatively wide range of matching tolerances that provide reasonably complete automatic assignment (0.2–0.6 ppm for heteronuclei) not only simplifies the use of RAVASSA for samples different from those studied here but also suggests its power for assignment of larger proteins (because assignment ambiguity is determined by matching tolerances and protein size).

Figure 5 summarizes the automatically obtained resonance assignment, which is evenly distributed among different structural elements of MBP. About 18% of α and amide ^1H remained unassigned, which are likely undetectable with CP-based methods because of either increased local dynamics or intermediate conformational exchange as suggested by peak counts in the triple resonance spectra (see the Supporting Information). In lieu of manual verification of the assignment, we performed an unbiased correlation of protein dihedral angles φ and ψ predicted by TALOS-N³⁹ on the basis of the automatically assigned shifts with respect to those in the X-ray derived structure (PDB 1ANF). A very good agreement (Figure 5D) proves validity of chemical shifts, whereas a very few outliers (1.5% of 470 angles) remain well within the limitations of TALOS predictions. We observe a very good match overall between the newly assigned chemical shifts and those of MBP in solution, at least for $^{13}\text{C}\alpha$ and $^{13}\text{C}\beta$ nuclei (Figure S13). Larger differences are observed for amide ^{15}N and ^1H , which are notoriously sensitive to the chemical environment, and vary significantly with the ligand complexation state of the protein and with preparations conditions (pH, buffer, and precipitant).

In comparison with assignment strategies developed for protein solutions, the solid-state samples present unique challenges. While in solution, a main limitation to tackling larger proteins arises because of the decreased sensitivity of slowly tumbling molecules, which is inherently dependent upon particle size. The size limit in solution can, to a certain degree, be extended by increasing temperature, reducing relaxation via deuteration, and implementing TROSY techniques, which select for long-lived spin components.⁴⁰ Although these issues are absent in the solid, the line widths of solid protein preparations are typically larger than those in solution, and unsurprisingly, the limitation in this case becomes resonance overlap and ambiguity in sequential resonance matching. (Even with the advantages of proton detection, the sensitivity at present limits acquisitions to 3D or 4D data sets, with 3D data being the most common.) The present approach using a large number of coacquired spectra meets these unique challenges encountered in solid protein preparations.

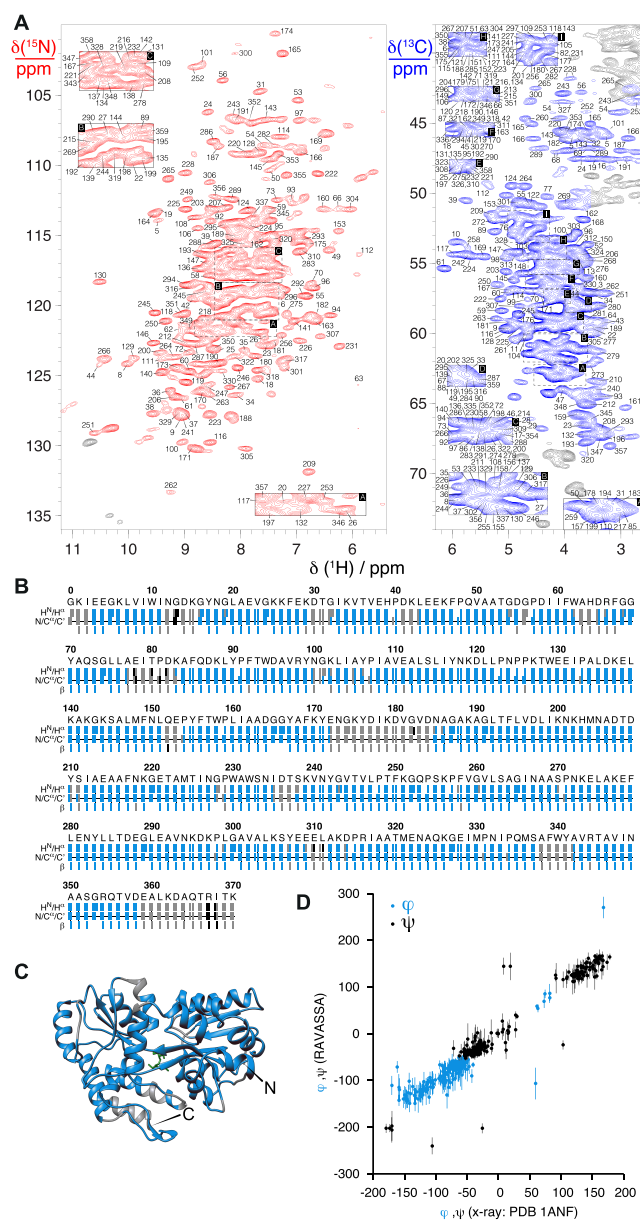


Figure 5. Assigned dipolar heteronuclear correlation spectrum of maltose binding protein: ^{15}N - ^1H (red contours) and α -region of ^{13}C - ^1H correlations (blue contours), acquired simultaneously. (B) Result of automated FLYA resonance assignment of MBP. Resonances with “strongly” determined chemical shifts are marked in blue (or in black, if located in isolated short fragments and thus discarded), whereas those below confidence threshold are shown in gray. (C) X-ray derived structural model of maltose binding protein (PDB 1ANF) with assigned residues marked in blue. (D) Backbone dihedral angles φ and ψ predicted on the basis of assigned chemical shifts and in the X-ray structure.

CONCLUSION

We have described a novel strategy for backbone NMR assignment of large proteins that does not rely on deuteration, but instead is based on automated analysis of high-resolution proton-detected 3D spectra obtained at ultrafast MAS with parallel $^1\text{H}^{\text{N}}$ and $^1\text{H}\alpha$ detection. We showed that full occupation of proton sites enables a simultaneous acquisition of six different correlation spectra, which offers significant time savings or, equivalently, sensitivity gains. Inherent consistency

and redundancy of the data provide an additional benefit to automatic resonance assignment of otherwise overwhelming complexity, as shown in the example of maltose binding protein (371 residues), which to our knowledge is the largest monomeric protein assigned in the solid state. A single uniformly ^{13}C , ^{15}N -labeled sample (<1 mg) and approximately 1 week of 800 MHz NMR instrument time, using a standard single receiver were used in this study. We furthermore showed that the assignment strategy is particularly robust against the choice of chemical shift matching tolerance, or line widths observed for a particular sample. We therefore expect that the approach will open an efficient avenue to access site-specific NMR information in large proteins, and will be readily extended to even larger proteins, or proteins exhibiting more challenging resolution.

EXPERIMENTAL SECTION

Sample Preparation. ^{13}C , ^{15}N -labeled N-terminal His-TEV-tagged maltose binding protein (MalE 27-396, *Escherichia coli*) was expressed in *E. coli* C41 cells and purified on a 5 mL Ni^{2+} -sepharose column (GE Healthcare) using standard methods. The His tag was removed with TEV-Protease (in-house production) and MBP was further purified by size-exclusion and ion-exchange chromatography. Eventually, the protein was dialyzed against 10 mM 4-(2-hydroxyethyl)-1-piperazineethanesulfonic acid (HEPES pH 7.5) and 1 mM maltose. Small platelet-like crystals were produced by sitting drop vapor diffusion in 24-well plates using 600 μL reservoir solution (10 mM HEPES pH 7.5 and 3 M $(\text{NH}_4)_2\text{SO}_4$). In each well, 15 μL of MBP solution ($c = 5$ mg/mL) was mixed with 15 μL reservoir solution. Crystals grew at room temperature within 3 days. One 24-well plate yielded sufficient material for one NMR sample. $(\text{NH}_4)_2\text{SO}_4$ was chosen as the precipitant (instead of, for example, PEG) to avoid introduction of naturally abundant ^{13}C nuclei. MBP crystals were packed by ultracentrifugation at 100000g at 10 $^\circ\text{C}$ directly into a 0.7 mm MAS rotor using a 1.3 mm ultracentrifuge tool (Giotto Biotech).⁴¹

NMR Spectroscopy. The experiments were performed on a Bruker AVANCE III 18.8 T spectrometer (^1H frequency of 800 MHz) using a 4-channel (HCND) 0.7 mm MAS probe. Sample rotation frequency was maintained at 107.00 ± 0.02 kHz, and the sample temperature was approximately 15 $^\circ\text{C}$. Details on RF applied during CP transfers, pulse program listings, and RF schemes are provided in the Supporting Information. All spectra were processed with nmrPipe⁴² using scripts provided in the Supporting Information, peak-picked automatically, and converted to Xeay format in CcpNmr Analysis 2.4.³⁴

SIM-CP Simulations. Simulations of simultaneous $^1\text{H} \rightarrow ^{13}\text{C}$, ^{15}N CP were performed with SIMPSON⁴³ software version 4.0.0c for rotation frequencies between 20 and 125 kHz. Powder averaging was performed with $168 \times 17 = 2856$ Euler angles $\{\alpha_{\text{MR}}, \beta_{\text{MR}}, \gamma_{\text{MR}}\}$, which described the orientation of the molecule in the rotor frame. One hundred sixty-eight angle pairs $\{\alpha_{\text{MR}}, \beta_{\text{MR}}\}$ were selected according to the Repulsion method,⁴⁴ whereas 17 γ_{MR} angles were regularly stepped from 0 to 360 $^\circ$. Seven spins were considered to simulate a proton bath in the fully protonated proteins: $^1\text{H}^{\text{N}}$, $^1\text{H}\alpha$, $^1\text{H}\beta_2$, $^1\text{H}\beta_3$, ^{15}N , $^{13}\text{C}\alpha$, and $^{13}\text{C}\beta$. The simulation was performed at 18.8 T magnetic field strength (^1H frequency of 800 MHz). The RF irradiation of ^{15}N , $^{13}\text{C}\alpha$ was considered on-resonance, $^{13}\text{C}\beta$ was assumed -20 ppm off-resonance, and $^1\text{H}^{\text{N}}$, $^1\text{H}\alpha$, and $^1\text{H}\beta_2/1\text{H}\beta_3$ chemical shift offset with respect to RF carrier (typically 4.7 ppm for solvent signal) was set to 4.0, -0.5 , and -2.2 ppm, respectively. Chemical shift anisotropy was neglected for all spins. RF irradiation strength ranges were 0–250 kHz for ^1H , ^{13}C , and ^{15}N . RF field inhomogeneity was neglected; thus, constant RF amplitude was assumed during CP. Only proton thermally equilibrated magnetization was considered at the starting point of the simulation. To simulate CP transfer, we calculated and reused the propagator for one rotor period to reach a contact time of 300 μs . The SIM-CP efficiency

was evaluated as the ^{15}N and $^{13}\text{C}\alpha$ magnetization at the end of RF irradiation. Further details, including the geometry of the restricted spin system and sample scripts, can be found in the [Supporting Information](#).

Automated Assignment. Automated analysis of the obtained correlations was performed by FLYA as implemented in CYANA package v. 3.98.5. Library extensions for new types of experiments as well as CYANA batch scripts are provided in the [Supporting Information](#). Optimal assignment was obtained using matching tolerances of 0.1, 0.3, and 0.3 ppm for ^1H , ^{13}C , and ^{15}N frequencies, respectively. A population size of 50 was set for a genetic optimization algorithm. Twenty independent runs were performed to identify consensus chemical shifts, with a threshold of 16 self-consistent chemical shift values for a “strong” assignment. Detailed statistics on the assignment completeness for particular nuclei and peak lists are provided in the [Supporting Information](#).

■ ASSOCIATED CONTENT

■ Supporting Information

The Supporting Information is available free of charge at <https://pubs.acs.org/doi/10.1021/jacs.0c00251>.

Detailed NMR experimental setup, radiofrequency irradiation schemes with Bruker spectrometer implementation, and details on data processing and automated analysis ([PDF](#))

■ AUTHOR INFORMATION

Corresponding Author

Guido Pintacuda – Centre de RMN à Très Hauts Champs (FRE 2034 CNRS, UCB Lyon 1, ENS Lyon), Université de Lyon, Villeurbanne 69100, France; orcid.org/0000-0001-7757-2144; Email: guido.pintacuda@ens-lyon.fr

Authors

Jan Stanek – Centre de RMN à Très Hauts Champs (FRE 2034 CNRS, UCB Lyon 1, ENS Lyon), Université de Lyon, Villeurbanne 69100, France; Faculty of Chemistry, University of Warsaw, Warsaw 02089, Poland

Tobias Schubeis – Centre de RMN à Très Hauts Champs (FRE 2034 CNRS, UCB Lyon 1, ENS Lyon), Université de Lyon, Villeurbanne 69100, France

Piotr Paluch – Faculty of Chemistry, University of Warsaw, Warsaw 02089, Poland

Peter Güntert – Physical Chemistry, Eidgenössische Technische Hochschule Zurich, Zurich 8093, Switzerland; Center for Biomolecular Magnetic Resonance, Institute of Biophysical Chemistry, Goethe University Frankfurt am Main, Frankfurt am Main 60438, Germany; Department of Chemistry, Tokyo Metropolitan University, Hachioji 192-0397, Japan

Loren B. Andreas – Centre de RMN à Très Hauts Champs (FRE 2034 CNRS, UCB Lyon 1, ENS Lyon), Université de Lyon, Villeurbanne 69100, France; Max Planck Institute for Biophysical Chemistry, Göttingen D-37077, Germany; orcid.org/0000-0003-3216-9065

Complete contact information is available at: <https://pubs.acs.org/doi/10.1021/jacs.0c00251>

Author Contributions

#J.S. and T.S. contributed equally to this work.

Notes

The authors declare no competing financial interest.

■ ACKNOWLEDGMENTS

The MBP plasmid was kindly provided by Prof. Gottfried Otting (ANU). The work was funded by the European Research Council (ERC) under the European Union’s Horizon 2020 research and innovation programme (ERC-2015-CoG GA 648974). J.S. was supported by the European Commission’s REA with a MSCA fellowship (GA 661799) and by the Polish National Agency for Academic Exchange (Contract No. PPN/PPO/2018/1/00098). The computational resources were provided by the Polish Infrastructure for Supporting Computational Science in the European Research Space (PLGRID).

■ REFERENCES

- (1) Barbet-Massin, E.; Pell, A. J.; Retel, J. S.; Andreas, L. B.; Jaudzems, K.; Franks, W. T.; Nieuwkoop, A. J.; Hiller, M.; Hignman, V.; Guerry, P.; Bertarello, A.; Knight, M. J.; Felletti, M.; Le Marchand, T.; Kotelovica, S.; Akopjana, I.; Tars, K.; Stoppini, M.; Bellotti, V.; Bolognesi, M.; Ricagno, S.; Chou, J. J.; Griffin, R. G.; Oschkinat, H.; Lesage, A.; Emsley, L.; Herrmann, T.; Pintacuda, G. Rapid proton-detected NMR assignment for proteins with fast magic angle spinning. *J. Am. Chem. Soc.* **2014**, *136*, 12489–12497.
- (2) Ishii, Y.; Yesinowski, J. P.; Tycko, R. Sensitivity enhancement in solid-state ^{13}C NMR of synthetic polymers and biopolymers by ^1H NMR detection with high-speed magic angle spinning. *J. Am. Chem. Soc.* **2001**, *123*, 2921–2922.
- (3) Reif, B.; Jaroniec, C. P.; Rienstra, C. M.; Hohwy, M.; Griffin, R. G. ^1H - ^1H MAS correlation spectroscopy and distance measurements in a deuterated peptide. *J. Magn. Reson.* **2001**, *151*, 320–327.
- (4) Paulson, E. K.; Morcombe, C. R.; Gaponenko, V.; Dancheck, B.; Byrd, R. A.; Zilm, K. W. Sensitive high resolution inverse detection NMR spectroscopy of proteins in the solid state. *J. Am. Chem. Soc.* **2003**, *125*, 15831–15836.
- (5) Zhou, D. H.; Shea, J. J.; Nieuwkoop, A. J.; Franks, W. T.; Wylie, B. J.; Mullen, C.; Sandoz, D.; Rienstra, C. M. Solid-state protein-structure determination with proton-detected triple-resonance 3D magic-angle-spinning NMR spectroscopy. *Angew. Chem., Int. Ed.* **2007**, *46*, 8380–8383.
- (6) Andreas, L. B.; Le Marchand, T.; Jaudzems, K.; Pintacuda, G. High-resolution proton-detected NMR of proteins at very fast MAS. *J. Magn. Reson.* **2015**, *253*, 36–49.
- (7) Böckmann, A.; Ernst, M.; Meier, B. H. Spinning proteins, the faster, the better? *J. Magn. Reson.* **2015**, *253*, 71–79.
- (8) Samoson, A. H-Mas. *J. Magn. Reson.* **2019**, *306*, 167–172.
- (9) Knight, M. J.; Webber, A. L.; Pell, A. J.; Guerry, P.; Barbet-Massin, E.; Bertini, I.; Felli, I. C.; Gonnelli, L.; Pierattelli, R.; Emsley, L.; Lesage, A.; Herrmann, T.; Pintacuda, G. Fast resonance assignment and fold determination of human superoxide dismutase by high-resolution proton-detected solid-state MAS NMR spectroscopy. *Angew. Chem., Int. Ed.* **2011**, *50*, 11697–11701.
- (10) Lewandowski, J. R.; Dumez, J. N.; Akbey, Ü.; Lange, S.; Emsley, L.; Oschkinat, H. Enhanced resolution and coherence lifetimes in the solid-state NMR spectroscopy of perdeuterated proteins under ultrafast Magic-Angle Spinning. *J. Phys. Chem. Lett.* **2011**, *2*, 2205–2211.
- (11) Andreas, L. B.; Jaudzems, K.; Stanek, J.; Lalli, D.; Bertarello, A.; Le Marchand, T.; Cala-De Paepe, D.; Kotelovica, S.; Akopjana, I.; Knott, B.; Wegner, S.; Engelke, F.; Lesage, A.; Emsley, L.; Tars, K.; Herrmann, T.; Pintacuda, G. Structure of fully protonated proteins by proton-detected magic-angle spinning NMR. *Proc. Natl. Acad. Sci. U. S. A.* **2016**, *113*, 9187–9192.
- (12) Struppe, J.; Quinn, C. M.; Lu, M.; Wang, M.; Hou, G.; Lu, X.; Kraus, J.; Andreas, L. B.; Stanek, J.; Lalli, D.; Lesage, A.; Pintacuda, G.; Maas, W.; Gronenborn, A. M.; Polenova, T. Expanding the horizons for structural analysis of fully protonated protein assemblies by NMR spectroscopy at MAS frequencies above 100 kHz. *Solid State Nucl. Magn. Reson.* **2017**, *87*, 117–125.

- (13) Marchanka, A.; Stanek, J.; Pintacuda, G.; Carlomagno, T. Rapid access to RNA resonances by proton-detected solid-state NMR at > 100 kHz MAS. *Chem. Commun.* **2018**, *54*, 8972–8975.
- (14) Penzel, S.; Smith, A. A.; Agarwal, V.; Hunkeler, A.; Org, M. L.; Samoson, A.; Böckmann, A.; Ernst, M.; Meier, B. H. Protein resonance assignment at MAS frequencies approaching 100 kHz: a quantitative comparison of J-coupling and dipolar-coupling-based transfer methods. *J. Biomol. NMR* **2015**, *63*, 165–186.
- (15) Andreas, L. B.; Stanek, J.; Le Marchand, T.; Bertarello, A.; Paepe, D. C.; Lalli, D.; Krejčíková, M.; Doyen, C.; Oster, C.; Knott, B.; Wegner, S.; Engelke, F.; Felli, I. C.; Pierattelli, R.; Dixon, N. E.; Emsley, L.; Herrmann, T.; Pintacuda, G. Protein residue linking in a single spectrum for magic-angle spinning NMR assignment. *J. Biomol. NMR* **2015**, *62*, 253–261.
- (16) Xiang, S.; Grohe, K.; Rovó, P.; Vasa, S. K.; Giller, K.; Becker, S.; Linsler, R. Sequential backbone assignment based on dipolar amide-to-amide correlation experiments. *J. Biomol. NMR* **2015**, *62*, 303–311.
- (17) Fricke, P.; Chevelkov, V.; Zinke, M.; Giller, K.; Becker, S.; Lange, A. Backbone assignment of perdeuterated proteins by solid-state NMR using proton detection and ultrafast magic-angle spinning. *Nat. Protoc.* **2017**, *12*, 764–782.
- (18) Wang, S.; Munro, R. A.; Shi, L.; Kawamura, I.; Okitsu, T.; Wada, A.; Kim, S.-Y.; Jung, K.-H.; Brown, L. S.; Ladizhansky, V. Solid-state NMR spectroscopy structure determination of a lipid-embedded heptahelical membrane protein. *Nat. Methods* **2013**, *10*, 1007–1012.
- (19) Retel, J. S.; Nieuwkoop, A. J.; Hiller, M.; Higman, V. A.; Barbet-Massin, E.; Stanek, J.; Andreas, L. B.; Franks, W. T.; van Rossum, B. J.; Vinothkumar, K. R.; Handel, L.; de Palma, G. G.; Bardiaux, B.; Pintacuda, G.; Emsley, L.; Kuhlbrandt, W.; Oschkinat, H. Structure of outer membrane protein G in lipid bilayers. *Nat. Commun.* **2017**, *8*, 2073.
- (20) Vasa, S. K.; Singh, H.; Rovo, P.; Linsler, R. Dynamics and Interactions of a 29 kDa Human Enzyme Studied by Solid-State NMR. *J. Phys. Chem. Lett.* **2018**, *9*, 1307–1311.
- (21) Ward, M. E.; Shi, L.; Lake, E.; Krishnamurthy, S.; Hutchins, H.; Brown, L. S.; Ladizhansky, V. Proton-detected solid-state NMR reveals intramembrane polar networks in a seven-helical transmembrane protein proteorhodopsin. *J. Am. Chem. Soc.* **2011**, *133*, 17434–17443.
- (22) Gauto, D. F.; Estrozi, L. F.; Schwieters, C. D.; Effantin, G.; Macek, P.; Sounier, R.; Sivertsen, A. C.; Schmidt, E.; Kerfah, R.; Mas, G.; Colletier, J. P.; Güntert, P.; Favier, A.; Schoehn, G.; Schanda, P.; Boisbouvier, J. Integrated NMR and cryo-EM atomic-resolution structure determination of a half-megadalton enzyme complex. *Nat. Commun.* **2019**, *10*, 2697.
- (23) Gupta, S.; Tycko, R. Segmental isotopic labeling of HIV-1 capsid protein assemblies for solid state NMR. *J. Biomol. NMR* **2018**, *70*, 103–114.
- (24) Han, Y.; Ahn, J.; Concel, J.; Byeon, I.-J. L.; Gronenborn, A. M.; Yang, J.; Polenova, T. Solid-State NMR Studies of HIV-1 Capsid Protein Assemblies. *J. Am. Chem. Soc.* **2010**, *132*, 1976–1987.
- (25) Stanek, J.; Andreas, L. B.; Jaudzems, K.; Cala, D.; Lalli, D.; Bertarello, A.; Schubeis, T.; Akopjana, I.; Kotelovica, S.; Tars, K.; Pica, A.; Leone, S.; Picone, D.; Xu, Z.-Q.; Dixon, N. E.; Martinez, D.; Berbon, M.; El Mammeri, N.; Noubhani, A.; Saupe, S.; Habenstein, B.; Loquet, A.; Pintacuda, G. NMR spectroscopic assignment of backbone and side-chain protons in fully protonated proteins: microcrystals, sedimented assemblies, and amyloid fibrils. *Angew. Chem., Int. Ed.* **2016**, *55*, 15504–15509.
- (26) Lalli, D.; Idso, M. N.; Andreas, L. B.; Hussain, S.; Baxter, N.; Han, S.; Chmelka, B. F.; Pintacuda, G. Proton-Based Structural Analysis of a Heptahelical Transmembrane Protein in Lipid Bilayers. *J. Am. Chem. Soc.* **2017**, *139*, 13006–13012.
- (27) Malmodin, D.; Papavoine, C. H.; Billeter, M. Fully automated sequence-specific resonance assignments of hetero-nuclear protein spectra. *J. Biomol. NMR* **2003**, *27*, 69–79.
- (28) Niklasson, M.; Ahlner, A.; Andresen, C.; Marsh, J. A.; Lundström, P. Fast and accurate resonance assignment of small-to large proteins by combining automated and manual approaches. *PLoS Comput. Biol.* **2015**, *11*, e1004022.
- (29) Gopinath, T.; Veglia, G. Dual acquisition magic-angle spinning solid-state NMR-spectroscopy: simultaneous acquisition of multi-dimensional spectra of biomacromolecules. *Angew. Chem., Int. Ed.* **2012**, *51*, 2731–2735.
- (30) Das, B. B.; Opella, S. J. Multiple acquisition/multiple observation separated local field/chemical shift correlation solid-state magic angle spinning NMR spectroscopy. *J. Magn. Reson.* **2014**, *245*, 98–104.
- (31) Linsler, R.; Bardiaux, B.; Higman, V.; Fink, U.; Reif, B. Structure calculation from unambiguous long-range amide and methyl 1H-1H distance restraints for a microcrystalline protein with MAS solid-state NMR spectroscopy. *J. Am. Chem. Soc.* **2011**, *133*, 5905–5912.
- (32) Gopinath, T.; Veglia, G. Orphan spin operators enable the acquisition of multiple 2D and 3D magic angle spinning solid-state NMR spectra. *J. Chem. Phys.* **2013**, *138*, 184201.
- (33) Sharma, K.; Madhu, P. K.; Mote, K. R. A suite of pulse sequences based on multiple sequential acquisitions at one and two radiofrequency channels for solid-state magic-angle spinning NMR studies of proteins. *J. Biomol. NMR* **2016**, *65*, 127–141.
- (34) Vranken, W. F.; Boucher, W.; Stevens, T. J.; Fogh, R. H.; Pajon, A.; Llinas, M.; Ulrich, E. L.; Markley, J. L.; Ionides, J.; Laue, E. D. The CCPN data model for NMR spectroscopy: development of a software pipeline. *Proteins: Struct., Funct., Genet.* **2005**, *59*, 687–696.
- (35) Schmidt, E.; Güntert, P. A new algorithm for reliable and general NMR resonance assignment. *J. Am. Chem. Soc.* **2012**, *134*, 12817–12829.
- (36) Schmidt, E.; Gath, J.; Habenstein, B.; Ravotti, F.; Székely, K.; Huber, M.; Buchner, L.; Böckmann, A.; Meier, B. H.; Güntert, P. Automated solid-state NMR resonance assignment of protein microcrystals and amyloids. *J. Biomol. NMR* **2013**, *56*, 243–254.
- (37) Pritišanac, I.; Würz, J. M.; Alderson, T. R.; Güntert, P. Automatic structure-based NMR methyl resonance assignment in large proteins. *Nat. Commun.* **2019**, *10*, 4922.
- (38) Barbet-Massin, E.; Pell, A. J.; Jaudzems, K.; Franks, W. T.; Retel, J. S.; Kotelovica, S.; Akopjana, I.; Tars, K.; Emsley, L.; Oschkinat, H.; Lesage, A.; Pintacuda, G. Out-and-back 13C-13C scalar transfers in protein resonance assignment by proton-detected solid-state NMR under ultra-fast MAS. *J. Biomol. NMR* **2013**, *56*, 379–386.
- (39) Shen, Y.; Bax, A. Protein backbone and sidechain torsion angles predicted from NMR chemical shifts using artificial neural networks. *J. Biomol. NMR* **2013**, *56*, 227–241.
- (40) Salzmann, M.; Pervushin, K.; Wider, G.; Senn, H.; Wüthrich, K. TROSY in triple-resonance experiments: new perspectives for sequential NMR assignment of large proteins. *Proc. Natl. Acad. Sci. U. S. A.* **1998**, *95*, 13585–13590.
- (41) Bertini, I.; Engelke, F.; Gonnelli, L.; Knott, B.; Luchinat, C.; Osen, D.; Ravera, E. On the use of ultracentrifugal devices for sedimented solute NMR. *J. Biomol. NMR* **2012**, *54*, 123–127.
- (42) Delaglio, F.; Grzesiek, S.; Vuister, G. W.; Zhu, G.; Pfeifer, J.; Bax, A. NMRPipe: a multidimensional spectral processing system based on UNIX pipes. *J. Biomol. NMR* **1995**, *6*, 277–293.
- (43) Bak, M.; Rasmussen, J. T.; Nielsen, N. C. SIMPSON: a general simulation program for solid-state NMR spectroscopy. *J. Magn. Reson.* **2000**, *147*, 296–330.
- (44) Bak, M.; Nielsen, N. C. REPULSION, A Novel Approach to Efficient Powder Averaging in Solid-State NMR. *J. Magn. Reson.* **1997**, *125*, 132–139.